Theoretical Chemistry Accounts (2022) 141:17
https://doi.org/10.1007/s00214-022-02871-z

REGULAR ARTICLE

Analyzing cases of significant nondynamic correlation with DFT using the atomic populations of effectively localized electrons

Conrad Lewis[1] · Emil Proynov[1,2] · Jianguo Yu[1] · Jing Kong[1,2]

Received: 13 September 2021 / Accepted: 23 January 2022 / Published online: 15 March 2022

Abstract
Quantum multireference effects are associated with degeneracies and near-degeneracies of the ground state and are critical to a variety of systems. Most approximate functionals of density functional theory (DFT) fail to properly describe such effects. A number of diagnostics have been proposed to estimate in advance the reliability of a given single-reference solution in this respect. Some of these diagnostics, however, lack size-consistency while remaining computationally expensive. In this work, we propose the DFT method of atomic populations of effectively localized electrons (APELE) as a novel diagnostic in this vein. It is compared with existing diagnostics of nondynamic correlation on select exemplary systems. The APELE method is on average in good agreement with the popular T_1 index, while being size-consistent and less costly. It becomes particularly informative in cases involving bond stretching or bond breaking. The APELE method is applied next to organic diradicals like the bis-acridine dimer and the p-quinodimethane molecule which possess unusually high nonlinear optical response, and to the reaction of ethylene addition to Ni dithiolene. Our results for this reaction are consistent with the T_1 diagnostics and in addition, shed some light on the degree of d-electron localization at the Ni center.

Keywords Density functional theory · Electron correlation · Chemical bonding

1 Introduction

In a typical theoretical study, one would start with some popular functional of density functional theory (DFT) or with a low level wavefunction-based correlation method and eventually would advance to the coupled cluster singles and doubles with perturbative triples (CCSD(T)) if the results are in doubt. These methods assume the dominance of a single-reference configuration (single-determinant- based methods). Single-determinant methods are unreliable for systems with strong multireference character in which more than one electronic configuration plays a significant role. The electron correlation due to multireference effects is called nondynamic correlation (NDC), and strong correlation when the NDC largely dominates. In multicenter systems, NDC tends to decouple a bond electron pair into two single unpaired electrons maximally separated from each other. This effect is also known as 'left–right' correlation [1–3]. The "simplest" example is the dissociating hydrogen molecule. At equilibrium, its two electrons with opposite spins are paired in a bond pair. Upon dissociation, the electrons become more and more "effectively unpaired" in the sense of virtual unpairing and localization on the H centers. This is due to the increased left–right correlation upon dissociation, which provides an energy gain by avoiding the two electrons to be close by. A proper description of this dissociation should take such a transformation into account without breaking the spin symmetry of the system.

Mainstream contemporary DFT functionals are known to poorly treat nondynamic/strong correlation, albeit some recent developments have shown great promise [4–9]. Instead, wavefunction-based methods like CASSCF (complete active space self-consistent field), MRCI (multireference configuration interaction), and their variations are usually employed. These methods are computationally expensive and can only be afforded to problems of relatively

Published as part of the special collection of articles "20th deMon Developers Workshop."

✉ Jing Kong
jing.kong@mtsu.edu

[1] Department of Chemistry, Middle Tennessee State University, Murfreesboro, TN 37132, USA

[2] Center for Computational Sciences, Middle Tennessee State University, Murfreesboro, TN 37132, USA

small size. It is desirable to be able to estimate a priori, the degree of multireference character of a given state, in order to estimate the reliability of a given single-determinant method. A few single-reference-based descriptors (diagnostics) have been proposed for this purpose. The most commonly used are based on CCSD(T), such as the T_1 [10], D_1 [11], and %TAE[12] indexes. These diagnostics estimate the strength of NDC in a system averaged way, averaging it per electron or per bond. However, NDC is often localized in specific subdomains of the system, like a transition-metal center in a complex or solid for example. In such cases, the NDC should remain approximately about the same upon increasing the system size by adding larger ligands for example, provided the latter does not change drastically the metal–ligand bonding pattern. Averaging the NDC over all electrons and/or bonds is not a size-consistent approach since some of these may not be directly involved in the multireference process. This leads to an artificial dilution of the NDC estimate.

Alternative methods of treating such effects in a local fashion have been developed, starting with the effectively unpaired ('localized', or 'odd') electron models of Takatsuka, Fueno and Yamaguchi [13], Lain et al. [14], Staroverov and Davidson [15], and Head-Gordon [16]. Upon stretching a bond, the bond electrons become partially decoupled due to the increased left–right NDC and tend to virtually localize as unpaired electrons on separate atoms. These electrons are referred to as 'effectively unpaired,' or 'effectively localized' electrons here. One example of effectively localized electrons are the electrons with radical character in diradicals. The above methods include, in principle, both nondynamic and dynamic correlation, while in fact localized radical density emerges mainly due to NDC. Recently, Ramos-Cordoba, Salvador and Matito [17] emphasized the importance of separating the electron correlation into dynamic and nondynamic parts and derived expressions of these, based on a cumulant expansion of the second-order reduced density matrix (RDM-2). These methods require correlated first-order reduced density matrix (RDM-1) which is not directly accessible from the single-determinant Kohn–Sham (KS) or Hartree–Fock (HF) solutions. More recently Liu, Duan and Kulik [18] proposed a local index of NDC based on a finite-temperature DFT formulation by Chai [19] that provides fractionally occupied orbitals and a non-idempotent RDM-1 beyond the standard KS method. Their approach is built on the earlier works of Matito and co's [17, 20], and Grimme and Hansen's [21], and is essentially similar to the 'odd electrons' approach, since both use the degree of non-idempotency of RDM-1 evaluated one way or another.

As an alternative, Nakano et al. [22] have proposed an index of diradical character (y) based on the HOMO–LUMO gap in natural-orbital representation of the spin-projected unrestricted self-consistent field (SCF) solution.

We have developed previously a DFT method of describing the formation of radical-like density [23]. It leads to a compact expression of the atomic population of effectively localized electrons (APELE) within a single-determinant KS DFT approach. The method retains the computational efficiency of a single-determinant KS solution while incorporating explicitly NDC in the evaluation of APELE. It does not involve fractional orbital occupancies, unlike the methods of refs. [18, 21], and is simpler to implement within the standard KS framework. Also, the calculations do not require spin-symmetry breaking, thus avoiding the side effects of spin contamination. By design, the APELE values reflect the strength of NDC locally which leads to size-consistent comparisons among systems of different size. A typical example is a singlet diradical, where two electrons with opposite spin, that formally would be paired in a bond pair, are in fact localized, each on a separate center. Larger APELE of the radical atoms reflect stronger NDC acting locally among the radical electrons. It requires two-reference configurations or more in a correlated wavefunction treatment of such a situation without spin-symmetry breaking.

Indeed, strong electron correlation manifests most notably in singlet diradical molecules. Much attention has been devoted recently to a particular class of organic diradicaloids that have unusually high nonlinear optical (NLO) response [24]. Molecular design of efficient NLO systems is a subject of intense research due to their importance for photonics and optoelectronics such as optical switches, 3D microfabrics, photodynamic therapy and others. Recent studies have shown that the degree of diradicaloid character in systems like diphenalenyls, π-electron systems involving imidazole rings and in other compounds that involve quinoid and benzenoid resonance structures like p-quinodimethane (PQM), is a key factor for the large second-order hyperpolarizability (γ) of these systems [22, 25–28]. Similar features have been found also in some graphene nanoflakes [29, 30].

2 The APELE method within the Kohn–Sham DFT

The formation of open-shell singlet systems is driven by strong left–right NDC that tends to partly decouple a covalent bond electron pair and form radical-like effectively localized electrons. This formation has been related to the non-idempotency of the correlated RDM-1 [13, 31]. At single-determinant SCF level (HF or KS), RDM-1 remains idempotent (integer orbital occupation numbers of 1 or 0) and APELE formation is not feasible at that level. We have proposed a way to remedy this situation without using fractional orbital occupancies [23]. The (non) idempotency condition of the RDM-1 $\gamma(\mathbf{r};\mathbf{r}')$ reads:

$$D_\sigma(\mathbf{r}) = \rho_\sigma(\mathbf{r}) - \int \gamma_\sigma(\mathbf{r};\mathbf{r}')\,\gamma_\sigma(\mathbf{r}';\mathbf{r})\mathrm{d}\mathbf{r}' \geq 0 \qquad (1)$$

where ρ_σ is the electron density of spin σ, D_σ is the APELE density per spin σ. The total density of effectively localized electrons D_u and the total number of these electrons, $\overline{N}_u$, are then given by:

$$D_u(\mathbf{r}) = 2\sum_\sigma D_\sigma(\mathbf{r}); \qquad \overline{N}_u = \int D_u(\mathbf{r})\,\mathrm{d}\mathbf{r} \tag{2}$$

At the single-determinant level (KS or HF), RDM-1 is idempotent meaning $D_\sigma \equiv 0$ everywhere as a limiting case of Eq. (1). We generalize the integrand of Eq. (1) by introducing a model effective exchange-hole that is otherwise compatible with the single-determinant KS scheme but having a specific form and relaxed normalization [23]:

$$\gamma_\sigma(\mathbf{r};\mathbf{r}')\gamma_\sigma(\mathbf{r}';\mathbf{r}) \approx \rho_\sigma(\mathbf{r})\,\overline{h}^{eff}_{X\sigma}(\mathbf{r},\mathbf{r}') \tag{3}$$

such that:

$$\int \overline{h}^{eff}_{X\sigma}(\mathbf{r},\mathbf{r}')\mathrm{d}\mathbf{r}' \le 1 \tag{4}$$

The existence of such a form was justified using an approximate cumulant expansion of the two-body density matrix [23]. In the APELE method, the effective exchange hole in Eq. (3) is represented by the relaxed exchange hole of Becke–Roussel [32] introduced in the B05 functional formalism [3, 33], $h^{B05}_{X\sigma}$, which estimates the NDC locally by its relaxed normalization $\overline{N}^{\mathrm{eff}}_{X\sigma}$ (similar to Eq. (4)):

$$\int h^{B05}_{X\sigma}(\mathbf{r},\mathbf{r}')\,\mathrm{d}\mathbf{r}' = \overline{N}^{\mathrm{eff}}_{X\sigma}(\mathbf{r}) \le 1 \tag{5}$$

The smaller the relaxed normalization $\overline{N}^{\mathrm{eff}}_{X\sigma}$, the stronger the NDC locally at a given reference point r. Using this relaxed exchange hole normalization in Eqs. (3),(1), the density of effectively localized electrons takes the form (see Appendix of ref. [23] for details):

$$D_u(\mathbf{r}) = 2\sum_\sigma \rho_\sigma(\mathbf{r})\left(1-\overline{N}^{\mathrm{eff}}_{X\sigma}(\mathbf{r})\right) \tag{6}$$

The smaller the relaxed normalization $\overline{N}^{\mathrm{eff}}_{X\sigma}$, the larger the density of effectively localized electrons.

To obtain the APELE of an individual atom A (denoted here as $F_r(A)$), we partition the molecular space into atomic regions (Ω_A) using the grid-based atomic partitioning of Becke's grid integration scheme [34].

$$F_r(A) = \int_{\Omega_A} D_u(\mathbf{r})\,\mathrm{d}\mathbf{r}, \quad \sum_A F_r(A) = \overline{N}_u \tag{7}$$

The values of the individual APELE, $F_r(A)$, and the sum of all APELE (total APELE $\overline{N}_u$), may be used as NDC diagnostics measuring the strength of NDC locally ($F_r(A)$) and globally ($\overline{N}_u$) per Eq. (7). The APELE density, Eq. (6), can be used to generate 2D and 3D plots illustrating the NDC distribution locally in the molecular space, similar to the plots presented in refs.[20, 21]. The APELE analysis was applied previously to elucidate more fully the bonding nature of Cr_2, C_2 and $(NO)_2$ dimer [23]. It was found that the bond in C_2 is unlikely to have diradical character in its ground state, while the singlet ground state of the $(NO)_2$ dimer does have a diradical character. The APELE method correctly estimated the magnetic moment localized on the Cr atoms in Cr_2 and predicted that the bond in Cr_2 may have a quad-radical nature [23]. It is worth reminding that the total APELE $\overline{N}_u$ is a quantum-statistical averaged number [14], in contrast to the total number of electrons in the system which is considered fixed here.

3 Computational details

The APELE-based NDC indexes were calculated with the KP16/B13 functional [5] which take into account NDC via real-space corrections to the exchange hole. This allows open-shell singlets to be described with restricted single-determinant KS (RKS) solution even at large bond stretches. This way we avoid the painful symmetry breaking procedure that is not always feasible.

Psi4, an open-source quantum chemistry software package [35], was used to optimize the structures at B3LYP/cc-pVQZ level using very tight convergence criteria. Psi4 was also used to evaluate the CCSD(T) diagnostics T_1, D_1, and %TAE[(T)], as well as, the A_λ diagnostic for M06, and M06-HF [35]. Instances in which the Psi4 package failed to deliver accurate results were circumvented using the Gaussian'09 software package [36]. The APELE results were obtained with the KP16/B13 functional using cc-pVTZ and G3LARGE basis sets [37] using the xTron code, an in-house computational program that allows the efficient computation of the HF exchange energy density [38–40]. It allows users to run various datasets with single commands in a cluster environment.

4 Diagnostics of nondynamic correlation

Wavefunction-based methods that include both dynamic and nondynamic correlation are expensive and quickly outscale the current computational resources. This motivated the need for diagnostic tools to predetermine whether NDC must be added to a given single-reference solution. There have been a number of techniques created for this purpose. They have been quite useful and have received wide popularity but often involve computationally complex methods

or require the help of other techniques. Here we give a gist of the more commonly used diagnostics that will next be compared with the proposed APELE-based diagnostics.

4.1 Summary of current diagnostics

4.1.1 Methods based on unrestricted SCF

Nakano et al. [22] have proposed an index of diradical character (y) based on the HOMO–LUMO gap in natural-orbital representation of the spin-projected unrestricted SCF (HF or Kohn–Sham) solution.

$$y = 1 - \frac{2T}{1+T^2}\ , \tag{8}$$

where T is the orbital overlap between the HOMO and LUMO natural orbitals. This analysis relies heavily on spin symmetry breaking, which brings large spin contamination. Moreover, a small HOMO–LUMO gap does not necessarily correspond to a large NDC, e.g., in a metallic system. Another problem is that systems with significant NDC do not always possess a spin-symmetry broken stable SCF solution with energy lowering.

4.1.2 CI based

The configuration interaction (CI) expansion of the wave function contains the expansion coefficients for each determinantal configuration involved. A system with a large amount of NDC would have a relatively small contribution to the total CI wave function from the main ground-state determinant. This diagnostic is represented by the leading coefficient (C_0) in the CI wave function expansion. It is quite informative, but it has an inherent bias tending to give higher C_0 values when the method uses single-determinant HF orbitals [41]. Complete Active Space SCF (CASSCF) calculations are used to remedy these shortcomings. It is generally accepted that a system with a $C_0 < 0.95$ or ${C_0}^2 < 0.90$ has multireference character and a multireference method should be used.

4.1.3 Coupled cluster based

The coupled cluster method employs a priori measures based on the $\vec{t}_1$ amplitudes and/or uses %TAE[(T)] (atomization energy due to triple excitations) as indicators of near-degeneracy. The Frobenius norm of the $\vec{t}_1$ amplitudes taken as a base and divided by the square root of the number of correlated electrons define the T_1 diagnostic [10]:

$$T_1 = \frac{\left\|\vec{t}_1\right\|}{\sqrt{n}} \tag{9}$$

The 'number of correlated electrons' n here implies only the valence electrons but not the core electrons. A few thresholds for T_1 have been suggested, which are largely based on the types of systems studied [10, 41] It is generally accepted that $T_1 > 0.02$ for organic molecules, $T_1 > 0.05$ for 3d transition metals, and $T_1 > 0.045$ for 4d transition metals indicates large NDC [41, 42].

Another diagnostic rooted in the coupled cluster approach is %TAE[(T)]. It uses the atomization energy from CCSD(T) compared with that from CCSD. This gives the percentage of atomization energy coming from the triple excitations alone:

$$\%\mathrm{TAE[(T)]} = \frac{\mathrm{TAE(CCSD(T))} - \mathrm{TAE(CCSD)}}{\mathrm{TAE(CCSD(T))}}\,100 \tag{10}$$

The %TAE[(T)] index is an energy-based diagnostic. It has been shown to correlate well with the more comprehensive estimates based on higher levels of the theory, such as $\%TAE[(T_4+T_5)]$ [41, 43]. %TAE[(T)] indicates mild, moderate, or strong NDC at less than 5%, greater than 5% but less than 10%, and greater than 10%, respectively [41]. This classification remains more or less consistent across the different types of systems.

4.1.4 DFT-based diagnostics

There are only a handful of methods developed for gauging NDC within DFT. The B_1 method developed by Schultz, Zhao and Truhlar has been shown to correlate well with the T_1 diagnostic for systems such as BeO and MgO [44]. Another diagnostic rooted in DFT that displays similar qualities is the A_λ diagnostic [43]. It uses the ratio of the atomization energy (AE) from a hybrid functional vs the atomization energy from 100% of HF exchange alone:

$$A_\lambda = \frac{\left(1 - \frac{\mathrm{AE}[(X_\lambda C)]}{\mathrm{AE}[(X_{100})]}\right)}{\lambda}, \tag{11}$$

where X and C denote here exchange and correlation components, respectively. The fraction of model DFT exchange $(100-\lambda)$ in the hybrid functional acts to some extent as a partial substitute for the left–right correlation. The fraction of HF exchange λ in the denominator of Eq. (11) normalizes this diagnostic.

For $A_\lambda < 0.10$, the system is primarily dominated by dynamic correlation, $A_\lambda \approx 0.15$ indicates that it is mildly ND correlated, $A_\lambda \approx 0.30$ means moderately ND correlated and for $A_\lambda > 0.50$ the system should be strongly ND correlated. It has been shown that A_λ agrees relatively well with %TAE[(T_4+T_5)] when certain specific functionals are used. A problem with the A_λ diagnostics is that the results sensibly depend on the approximate functionals used, and also that it is a system averaged index prone to size inconsistency.

Recently a DFT-based local indexes of NDC [21] has been proposed based on a finite-temperature DFT [19]. The main ingredients of this method are the electronic temperature T_{el} and the fractional occupations f_i of the temperature-dependent one-electron states governed by the Fermi–Dirac statistical distribution:

$$f_i = \frac{1}{e^{(\varepsilon_i - E_F)/kT_{\mathrm{el}}} + 1}, \quad 0 \le f_i \le 1 \tag{12}$$

Using this formalism, they proposed the so-called fractional orbital density (FOD) as a local index of NDC:

$$\rho^{\mathrm{FOD}}(\mathbf{r}) = \sum_i^N (\delta_1 - \delta_2 f_i)\left|\varphi_i(\mathbf{r})\right|^2, \tag{13}$$

where δ_1, δ_2 are constants chosen so that only the fractionally occupied orbitals are included in $\rho^{\mathrm{FOD}}(\mathbf{r})$. Although physically appealing, there seems no quite clear connection between this FOD density of 'hot' electrons and the strength of the NDC as defined within the zero-temperature quantum mechanics.

Another local index was more recently introduced and explored in refs. [17, 20] based on natural orbitals cumulant expansion of RDM-2 and its decomposition of dynamic and nondynamic correlation parts. The correlation part was written in terms of (spin-dependent) fractional occupation numbers (FON) n_i^σ of the natural spin orbitals ϕ_i^σ:

$$I_{\mathrm{ND}}(\mathbf{r}) = \frac{1}{2}\sum_{i,\sigma} n_i^\sigma (1 - n_i^\sigma)\left|\phi_i^\sigma\right|^2 \tag{14}$$

Equation (14) is in fact equivalent to the natural orbital representation of the 'effectively unpaired' ('odd') electron density defined via the non-idempotency of RDM-1 [13, 16]. Both expressions are a different way of representing the APELE density given by the real-space Eq. (6) [23] (see paragraph 2 and Sect. 4.2).

Very recently Liu, Duan and Kulik [18] combined Eq. (14) with the finite-temperature DFT expression (12) to obtain more efficient and easier to use DFT variant of the FON method. None of these latter methods introduce any quantitative atomic population analysis based on the FOD or FON local functions.

4.2 Diagnostic based on the atomic population of effectively localized electrons (APELE)

A brief gist of the APELE method is given in Sect. 2. Summing the APELE of all the atoms of the system gives the total APELE index $\overline{N}_u$, Eq. (7). Given the specific setup of our model, $\overline{N}_u$ reflects the global strength of NDC in the system and can be used as global NDC diagnostic complementing the APELE density distribution D_u, Eq. (6), and the individual APELE $F_r(A)$, Eq. (7). Indexing the NDC based on the APELE analysis ($F_r(A)$ and $\overline{N}_u$) has some distinct advantages. Above all, $F_r(A)$ is a local characteristic and does not include averaging over the whole system like in the case of T_1 or %TAE. Another advantage is the computational efficiency since our method is based on single-determinant KS-DFT and does not require fractional orbital occupancies. Furthermore, the method directly accounts for the NDC by design, so that the APELE values directly reflect the strength of NDC locally ($F_r(A)$) or globally ($\overline{N}_u$), and do not include contributions from dynamic correlation.

4.2.1 Linear alkane chains with a stretched central C–C bond distance

A good example illustrating the size-consistency issue is a set of linear alkanes with a stretched carbon–carbon bond in the middle [21]. The APELE results for ethane (C2H6), butane, (C4H10), hexane (C6H14) and octane (C8H18) are presented in Fig. 1 and Table 1.

Table 1 also contains the values of several other diagnostics calculated as explained in the computational details. The molecular geometries are first optimized with B3LYP/ cc-pVQZ. Then, the middle C–C bond ('C1–C2') is stretched out, starting from equilibrium (which for these systems is at around 1.5Å), up to 3.5Å. The bond stretching induces strong left–right ND correlation mainly localized at the C1–C2 bond of each molecule. Figure 1 shows the change of APELE on one of the two central carbon atoms in each alkane with increasing the C1-C2 distance. The observed trend is consistent with one's physical intuition that the NDC should increase when the bond is progressively stretched. This trend holds steady, and the values only slightly vary from ethane to octane, showing that the APELE index is size-consistent and reflects the increase in left–right correlation mainly at the C1–C2 bond. The coupled cluster-based diagnostics show the proper trend as the C1-C2 bond distance increases in each of the molecules. However, as we move from smaller to larger alkanes, the T_1, and %TAE[(T)] values tend to decline when comparing them at the same C1–C2 distance. As the size of the molecule increases, the values of these diagnostics become more diluted, which is a sign of size-inconsistency. A similar trend with the coupled

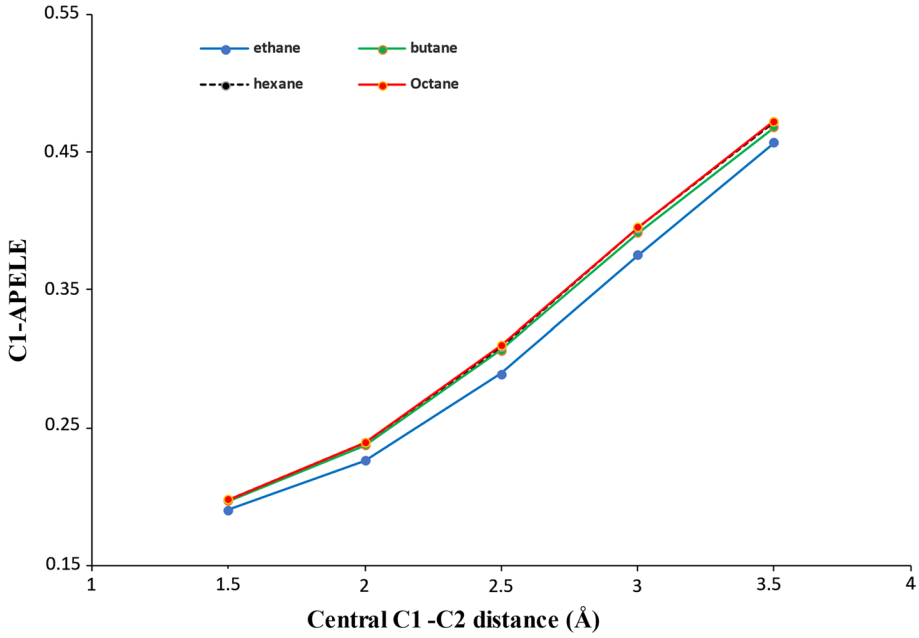

Fig. 1 APELE of the central C1 atom in the alkanes as a function of the C1-C2 distance

Table 1 Left–right correlation diagnostics. The APELE values are per C atom of the central C1-C2 bond

Molecule	Diagnostic	1.5Å	2.0Å	2.5Å	3.0Å	3.5Å
Ethane	APELE	0.1905	0.2262	0.2894	0.3754	0.4567
	T_1	0.0036	0.0088	0.0185	0.0340	0.0312
	%TAE[(T)]	−0.0501	0.1946	1.3395	2.9680	4.7210
	A_λ[M06]	−0.0088	−0.0086	0.0021	0.0174	0.0297
	A_λ[M06-HF]	−0.0059	−0.0077	0.0019	0.0204	0.0407
Butane	APELE	0.1968	0.2374	0.3061	0.3912	0.4679
	T_1	0.0041	0.0074	0.0156	0.0350	0.0437
	%TAE[(T)]	0.0242	0.1819	1.0212	1.9267	2.2979
	A_λ[M06]	−0.0079	−0.0043	0.0034	0.0118	0.0180
	A_λ[M06-HF]	−0.0060	−0.0050	0.0012	0.0104	0.0199
Hexane	APELE	0.1978	0.2391	0.3089	0.3950	0.4722
	T_1	0.0043	0.0068	0.0152	0.0150	0.0188
	%TAE[(T)]	0.0567	0.1773	0.7456	1.0377	1.7525
	A_λ[M06]	−0.0077	−0.0053	−0.0001	0.0054	0.0095
	A_λ[M06-HF]	−0.0058	−0.0056	−0.0018	0.0042	0.0105
Octane	APELE	0.1979	0.2394	0.3098	0.3956	0.4725
	T_1	0.0044	0.0063	0.0131	0.0132	0.0151
	%TAE[(T)]	0.0743	0.1692	0.5989	0.8045	1.2862
	A_λ[M06]	−0.0075	−0.0057	−0.0017	0.0025	0.0056
	A_λ[M06-HF]	−0.0057	−0.0054	−0.0025	0.0020	0.0067

cluster-based diagnostics on other occasions was reported in the literature as well [45].

Regarding the A_λ method, the M06, and M06-HF functionals were used for the evaluation of this index. These functionals include a fraction of 27% and 100% Hartree–Fock exchange, respectively. The obtained A_λ values all fall below the threshold suggested by the authors of ref. [43], and misleadingly would indicate that no significant NDC is present in these molecules at any bond stretch. However, the A_λ index does display qualitatively a proper trend with respect to the bond stretching. Similar to the coupled cluster-based diagnostics, the A_λ diagnostic is not size-consistent and reflects the situation is a system averaged way (see Eq. (11)).

To compare more fully the different diagnostics, a statistical correlation analysis was done on the results for the

Table 2 Correlation (in %) between the diagnostics at the equilibrium and at stretched C1-C2 bond length across all four alkanes

	Method	APELE	T_1	TAE[(T)]	A_λ[M06]
(a) C1–C2 = 1.5Å	T_1	97.214			
	%TAE[(T)]	96.765	99.982		
	A_λ[M06]	99.084	99.477	99.269	
	A_λ[M06-HF]	44.864	64.030	65.461	55.943
(b) C1–C2 = 3.5Å	T_1	−47.501			
	%TAE[(T)]	−99.322	44.655		
	A_λ[M06]	−97.176	64.709	97.107	
	A_λ[M06-HF]	−99.371	54.429	99.319	99.103

considered four alkanes. Table 2 contains the statistical correlation between the methods with respect to the trend of NDC in these alkanes. A relatively good agreement between the diagnostics is observed when the molecules are at their equilibrium geometry (small NDC, Table 2a), with an exception of A_λ[M06-HF]. The poor correlation of the latter with the rest of the diagnostics at equilibrium deserves more attention. Using 100% HF exchange in the M06-HF hybrid functional in the context of its multiparameter optimization leaves the A_λ[M06-HF] estimates without any simulation of NDC due to the lack of a model DFT exchange in the mixture. This is the main reason the A_λ[M06-HF] would correlate poorly with the rest of the diagnostics.

While most of the methods perform well at equilibrium here, the statistical analysis at C1-C2 = 3.5 $\mathring{A}$, Table 2b, shows a lack of size-consistency by all the methods but APELE, with high negative correlations with respect to the correct trend.

We have also calculated the total APELE index $\overline{N}_u$ for a few selected molecules from the W4-11 database [12] (Table 3). It is interesting that the two global indexes $\overline{N}_u$ and %TAE[(T)] agree well qualitatively when comparing molecules with the same stoichiometric composition. Table 3 lists four pairs of such molecules. For each pair, the total APELE index $\overline{N}_u$ is larger whenever %TAE is larger.

To keep in mind that in most singlet cases the $\overline{N}_u$ values have an upper limit of 2 here (diradical molecules), and that values of $\overline{N}_u$ below 0.15 are typical for singlet single-bonded molecules like H_2 at equilibrium.

4.2.2 Strength of NDC in acetylene vs vinylidene.

To extend the comparison among the different diagnostics, we consider next a pair of interesting molecules presented in Fig. 2 [46]. They are rather different in their properties but have formally the same stoichiometry. This allows a comparison of the relative strength of NDC in both structures using the individual APELE values as well as the total APELE index $\overline{N}_u$. For instance, the carbon atoms in acetylene have relatively stronger NDC than either of the carbons in vinylidene, while APELE of the hydrogen atoms vary only slightly. The total APELE index $\overline{N}_u$ for acetylene and vinylidene is 0.800 and 0.690, respectively, while the %TAE[(T)] values are 2.1 and 1.9. This confirms that $\overline{N}_u$ for relatively small systems with the same stoichiometry correlates well qualitatively with the wave-function-based diagnostics.

5 Other exemplary applications of the APELE method

5.1 Study of bis-acridine dimers

An interesting case study are the bis-acridine dimers considered by Nakano et al.[25]. The diradical character of these compounds has been verified and is analyzed here by applying the diagnostics to the Model 8 and Model 12 compounds considered in ref. [25]. All calculations are done at B3LYP/6-31G* optimized geometries. The only difference between the two compounds is that Model 8 has a positive charge of 2 while Model 12 is neutral [25]. Both molecules have a singlet ground state. Model 8 has been shown to have strong diradical character and high

Table 3 Calculated total APELE $\overline{N}_u$ vs the %TAE[(T)] index of selected small molecules

Molecule	C2H2	CH2C	c-HCOH	t-HCOH	c-HONO	t-HONO	H2C2O	H2CCO
$\overline{N}_u$	0.8003	0.6898	0.7272	0.7117	1.2895	1.3062	1.1754	1.1636
%TAE[(T)]	2.10	1.90	2.30	2.28	5.30	5.40	3.2	2.5

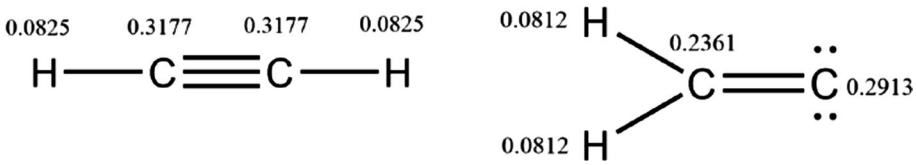

Fig. 2 Comparison of APELE in acetylene (left) vs vinylidene molecules

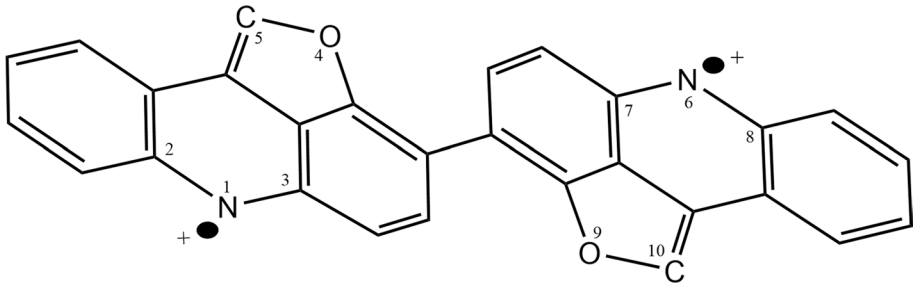

Fig. 3 A slightly simplified structure of Model 8 used in the calculations

Table 4 Calculated APELE values of the atomic groups in Model 8 carrying most of the radical density

HN1, HN6	C2, C8	C3, C7	O4,O9	C5,C10
0.457	0.284	0.294	0.432	0.324
Group total:	1.035		0.756	

second-hyperpolarizability corresponding to high intensity of the two-proton absorption. Figure 3 shows our slightly simplified structure used for Model 8 (and similarly for Model 12) in our calculations. The obtained total APELE values $\overline{N}_u$ are 12.834 and 12.281 for Model 8 and Model 12, respectively, indicating that Model 8 may involve larger NDC than Model 12. However, in these systems size-consistency matters since the radical density formation is localized about certain sub-regions of these molecules. The spin-density distribution calculated in ref. [25] for Model 8 with spin-symmetry breaking is mainly localized on the two N atoms and their nearest neighbors, all carrying the bulk of the positive charge and radical charge altogether. Our APELE results are in good agreement with the findings of Nakano et al., even though we do not use spin-symmetry breaking. Table 4 contains the APELE of the atoms that are carrying most of the diradical formation: (HN1 + C2 + C3) on one side (the N atom with its nearest neighbors, see Fig. 3) and their symmetric counterparts (HN6 + C7 + C8) on the other side, each group carrying a total of 1.035 unpaired radical charge. We also find some noticeable accumulation of APELE around each of the two oxygen atoms (O4 + C5 = 0.76 = O9 + C10) (Table 4), each oxygen being situated on the symmetrically opposite side of the N atoms. This indicates a possibility for tetra-radical formation in this compound or at least that NDC has an increased significance in the vicinity of these oxygens too. Once more, the ability of probing the strength of NDC locally/regionally within a given system brings some more detailed insight.

5.2 Study of the model system PQM

Much attention has been devoted to a particular class of organic diradicals with an unusually high nonlinear optical (NLO) response [22, 24, 27]. Recent studies have shown

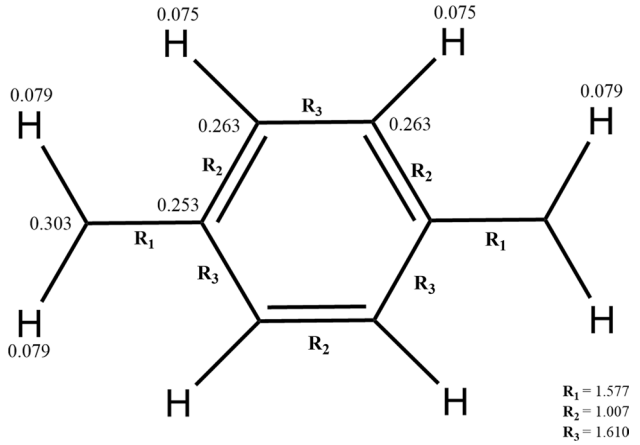

Fig. 4 The PQM structure optimized with B3LYP using G3LARGE basis set and (128,302) unpruned grid. The APELE values are also given

that the degree of diradical character in systems like p-quinodimethane (PQM) is related to the large second-order hyperpolarizability (γ) observed in these systems [22, 25–28].

The PQM (Fig. 4) system was studied first by Nakano and collaborators using their *y*-factor index (see Eq. (8)) in search for a connection between the degree of diradical character and the second hyperpolarizability [22]. Our APELE analysis allows to explore from somewhat different angle the strongly correlated nature of these NLO active diradicaloids. The p-quinodimethane (PQM) is an interesting example itself of a normal singlet state at equilibrium that transforms into an open-shell singlet upon stretching of certain key bonds. First we optimized the geometry of the PQM with B3LYP following the recommendation of ref.[22]. The lowest-energy geometry obtained with B3LYP has a typical alternating C–C bond pattern in the ring, similar to the one reported in ref.[22]. Bond length alternation in carbon ring systems is a known indication of π-electrons localization on the individual C–C bonds. This localization is sustained by strong ND left–right correlation. Similar effects have been observed in other polycarbonic systems [47], and in periodic systems [48]. In PQM, this effect is accompanied with loss of aromaticity, which is observed also in other carbon

Table 5 APELE of individual atoms and groups in the PQM diradicaloid

R_1	R_2	R_3	$F_r(CCH_2)$	$F_r(C_1)$	$F_r(C_2)$	$F_r(C_9H)$	$\overline{N}_u$	Q_r	y [c]
1.348 (eq) (1.351[a])	1.457 (eq) (1.460[a])	1.343 (eq) (1.346[a])	0.715 [0.713[b]]	0.253 [0.255[b]]	0.303 [0.301[b]]	0.338 [0.339[b]]	2.78	0.514	0.146
1.4	1.4	1.4	0.767	0.250	0.348	0.269	2.92	0.525	0.335
1.5	1.4	1.4	0.854	0.264	0.390	0.346	3.06	0.558	0.491
1.6	1.4	1.4	0.905	0.278	0.435	0.349	3.21	0.564	0.626
1.7	1.4	1.4	0.981	0.294	0.482	0.349	3.36	0.584	0.731
1.8	1.4	1.4	1.057	0.309	0.530	0.350	3.52	0.601	
2.0	1.4	1.4	1.206	0.342	0.621	0.350	3.81	0.633	

[a]Equilibrium geometry estimates of ref. [22]; [b]APELE values obtained perturbatively based on RB3LYP SCF solution, to compare with the APELE obtained self-consistently with KP16/B13. [c]The y values are from ref.[22]. The series of PQM geometries follow the pattern given in ref.[22]: R_1, R_2, R_3 are the three key bond distances in PQM, one of which, R_1, is gradually stretched in a symmetric fashion from both sides of the ring, See Fig. 4

ring systems with alternating C–C bond lengths [47]. Our results presented in Table 5 show that the PQM diradical charge estimated by APELE is partly delocalized around the C manifold, with an emphasis on the two terminal C-CH_2 group of atoms. It gradually increases with the symmetric stretch of the C–CH_2 bond distance on both sides of the ring. More pronounced is the change of the group-APELE Fr(C–CH_2), which shows that the increased NDC upon bond stretching is mainly confined locally within these group of atoms where the bond stretching occurs. The global NDC index $\overline{N}_u$ is relatively less sensitive to the stretching here, which shows again the importance of examining the effect of NDC locally.

Considering the diradical formation upon bond-stretching, a few DFT indexes have been proposed based on UKS calculations with broken spin-symmetry [22, 27, 28]. The y index was mentioned already (Eq. (8)). A difficulty with this approach is that not always the UKS or UHF calculations lead to a lower energy state with broken symmetry and localized radical spins. For example, we performed a stability analysis of the RKS vs UKS state of the PQM using RB3LYP and UB3LYP, respectively. At the equilibrium PQM geometry, there is no RKS-UKS instability of any kind, and the ground-state energy remains RKS. Our APELE analysis on the other hand shows that there is a good amount of NDC as evidenced by the $\overline{N}_u$ value of 2.78. In this case, one can hardly claim a diradical formation based on the UKS treatment alone, even though the y parameter value is also nonzero (Table 5) True RKS-UKS instability appears only when both C-CH_2 bond lengths are stretched to about 1.6 Å or so and longer.

Another group-APELE index in the case of PQM that shows a relative concentration of radical charge on the terminal C-CH_2 groups is $Q_r = 2(F_r(CCH_2)/\overline{N}_{u,}$ where $F_r(CCH_2)$ is the group-APELE in the union of these four atomic regions as mentioned above, Fig. 4. These are the atoms of the C-CH_2 fragment where most of the APELE charge is located. At equilibrium geometry, our estimate of Q_r here is about 0.514. It gradually increases to about 0.633 at stretched C-CH_2 distance of 2.0 Å. It is worth noting that the total number of radicalized electrons $\overline{N}_u$ is larger than 2 even at equilibrium. This is because there is some APELE located also on other C atoms from the ring, besides the diradical formation (Fig. 4). This is mainly due to the above-mentioned localization of the ring π electrons. Those findings are not accessible from the values of the global y index alone presented in Table 5.

5.3 Study of the ethylene addition to Ni dithiolene reactions

Metal bis(dithiolene) complexes have been widely studied because of their unusual chemical, redox, and optical properties related to the specific nature of the dithiolene ligand [49, 50, 51, 52]. Their complex character makes it difficult to assign unambiguously the oxidation state of the metal center, as pointed out in the studies of Dang et al.[53] on the transition states and intermediates of the ethylene addition to Ni(edt)$_2$ (edt = $S_2C_2H_2$). A wide variation of calculated relative reaction and transition-state energies using different functionals has been reported, which was attributed mainly to the peculiar multireference character of the Ni-ligand bonding in these systems. The latter was confirmed both experimentally and by the reported T_1 diagnostic of the different reaction species and CASSCF relative energies [53].

We apply here the APELE analysis to estimate the degree of radical character of these reaction species in the notations of ref [53]. (see Figs. 5,6). Large APELE values also mean

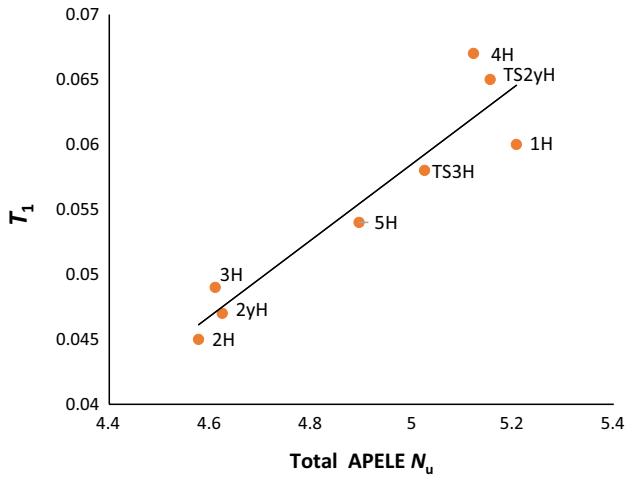

Fig. 5 Correlation between $\overline{N}_u$ and T_1 for the different reaction species

that the corresponding atoms are less involved in normal covalent bonding while they may remain highly reactive due to their unpaired radical-like electrons. The comparison between the $\overline{N}_u$ and T_1 diagnostics in this case shows a relatively good correlation between the two (Fig. 5).

The variations among different reaction species can be further analyzed based on the total APELE value $\overline{N}_u$ and the individual or group APELE values which are not available from the T_1 analysis alone. The results from the APELE analysis on some of the reaction species (the initial reactant 1H and the product 2H, Fig. 6) are summarized in Table 6. We observe a large decrease of APELE on the two upper S atoms (S1, S3, Fig. 6) when going from 1H to 2H reaction species. This is due to their bonding with the carbon atoms of ethylene in the 2H product. These new S–C bonds cause in turn some decrease of APELE on the Ni center, which means that a fraction of APELE on Ni in 1H is now engaged in enforcing the Ni-S bonds in 2H. Hence, we observe some decrease of the radical-like density on the Ni center when going from the initial 1H structure to the 2H product.

More detailed studies of the electronic aspects of this reaction are in order, particular concerning the evolution of the oxidation state of the Ni center along the reaction path. A lot has already been done along these lines (see ref [53]. and references therein). Testing our APELE-based indexes of NDC in this case shows an encouraging agreement with the T_1 diagnostic and yields some additional information not directly assessable by the T_1 diagnostic alone (Table 6).

5.4 Study of multireference character of transition-metal compounds

A variety of materials contain transition metal (TM) elements as essential ingredients. Those compounds often have moderate-to-strong multireference character mainly due to the partly filled inner d-shells of the TM centers. The APELE method could be advantageous in studies of such compounds. We are currently exploring this possibility using the ccCA-TM-11 (correlation-consistent composite approximation for transition-metals 2011) database [54]. The multireference character of these complexes has been examined already by the same authors using the T_1, %TAE, and a few other diagnostics based on CASSCF [41]. It is still a work in progress from our side. Here we present just a small exemplary case of transition-metal-carbonyl complexes that have interesting bonding features. Table 7 lists the calculated APELE values of Ni and Cr in small series of their carbonyls. All these molecules are singlets (low-spin complexes). The metal–ligand bonding here is different from the bonding in organic diradicals

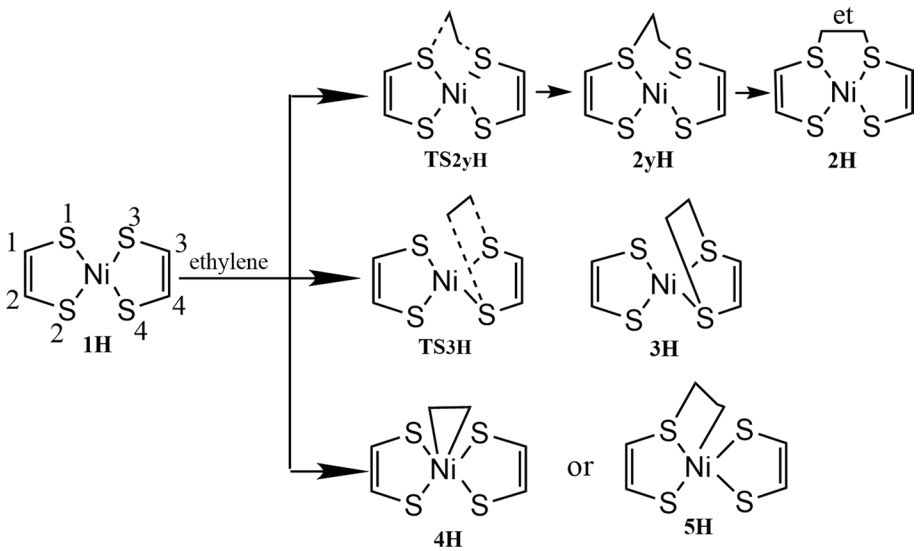

Fig. 6 Reaction species in the ethylene addition to Ni dithiolene reactions per ref. [53]

Table 6 APELE values of the atoms in the 1H and 2H reaction species in the reaction of ethylene addition to $Ni(edt)_2$

	APELE	APELE	APELE
Atoms	1H	2H	2H–1H
Ni	0.666	0.563	− 0.104
S3	0.503	0.374	− 0.129
S2	0.503	0.463	− 0.040
S1	0.503	0.374	− 0.129
S4	0.503	0.462	− 0.041
C2	0.338	0.315	− 0.023
C3	0.338	0.298	− 0.040
C4	0.338	0.314	− 0.024
C1	0.338	0.300	− 0.039
C(et)	0.242[a]	0.207	− 0.035
C(et)	0.242[a]	0.211	− 0.031

[a] APELE of the C atoms in isolated ethylene

Table 7 Calculated APELE values on Ni and Cr in a series of carbonyl complexes. The T_1 and %TAE values are from ref.[41]

Molecule	APELE	%TAE	T_1
NiCO	0.63	11.1	0.046
$Ni(CO)_2$	0.67	7.5	0.037
$Ni(CO)_3$	0.66	6.4	0.031
$Ni(CO)_4$	0.69	6.1	0.031
$Cr(CO)_3$	0.97	6.5	0.054
$Cr(CO)_4$	0.96	5.8	0.036
$Cr(CO)_5$	0.95	5.5	0.032
$Cr(CO)_6$	0.94	5.3	0.028

and acquires a multicenter character upon increasing the number of ligands. The bonding of a given CO ligand to the transition metal center is done via the CO carbon atom. The lone electron pair of the ligand carbon atom induces a donation of electron density to the empty metal d-orbitals, forming a dative bond. The donated electron density enhances the energy of the metal d-electrons due to increased electron–electron repulsion. This in turn facilitates a π-acceptor bonding interaction between the metal d-electrons and the empty π* orbitals of the CO ligand. Such a two-process picture of the metal–ligand bonding shows a possibility of significant left–right correlation due to the rather localized nature of the metal d-electrons. The APLELE of the TM atoms reflects this localization and hence the left–right correlation between the metal and the ligand electrons.

The %TAE and T_1 values tend to decrease when more ligands are added to the Ni complex, which is in part due to the size inconsistency issue with these diagnostics. The APELE values on the other hand remain almost constant (a slight increase in the second decimals) for the Ni series. A decreasing pattern of the CC-based indexes is also observed in the Cr-based complexes when number of the ligands increases. The APELE values again remain almost unchanged in his case too, with a very slight decrease in the second decimals upon increasing the number of ligands.

Both APELE and T_1 show an increased multireference character going from $Ni(CO)_3$ to $Cr(CO)_3$ complex. This is mainly due to the difference in the metal electronic configuration in these two complexes, particularly in regard to the partly filled inner 3d shell ($Ni(3d^8)$ vs. $Cr(3d^5)$) which results in different strength and bond order of the metal–ligand bonding. APELE maintains essentially the same difference between the larger $Ni(CO)_4$ and $Cr(CO)_4$ complexes while the difference in T_1 is smaller there, perhaps due to the increase of molecular size.

The distinction between these two types of complexes with the same number of ligands is less clear from the %TAE values.

6 Conclusions

Nondynamic correlation plays an important role in many cases, but it is expensive and hard to take into account. Most approximate DFT functionals fail to describe it properly. A number of diagnostics have been proposed that allow to estimate the quality of a given single-reference solution in this respect. Most of these diagnostics are, however, not size-consistent, while remaining computationally expensive. In this work, we use our DFT method of atomic population of effectively localized electrons (APELE) and the total number of effectively localized electrons [23] as novel diagnostics in this vein. It retains the simplicity of the single-determinant Kohn–Sham DFT in contrast to some more recent methods based on explicit fractional orbital occupancy [18, 21]. The APELE analysis is generally in good agreement with other currently used diagnostics like T_1 and %TAE, while having the advantage of being size-consistent, less costly and does not involve unrestricted spin-symmetry breaking. It becomes particularly informative in cases involving bond stretching or bond breaking as in the series of linear alkane chains. The APELE method is used also to explore some specifics of organic diradicaloids like the bis-acridine dimer and the p-quinodimethane having unusually high nonlinear optical response. The calculated APELE values point out on nonnegligible nondynamic correlation in these systems that is localized within certain specific subdomains of the molecules. We tested the method also on the complicated reaction of ethylene addition to Ni dithiolene that was already studied before with the T_1 diagnostic. The results

with APELE are consistent with that of T_1, with additional atomic detail on how the degree of d-electron localization on the Ni center may change when going from the initial reactant to the final product.

Acknowledgements JK thanks Dr. Pachter for very helpful discussions on the topic of this paper. He also thanks Dr. Hall for discussions on the Ni dithiolene reactions. The authors thank Drs. Liu, Wang and John for assistance. EP thanks Dennis Salahub for the long years of mentorship, friendship and support. This work received support from Air Force Research Laboratory of US Department of Defense under the AFRL Minority Leaders—Research Collaboration Program, contract FA8650-13-C-5800 (Clearance Authority: 88ABW-2016-5818), and from the National Science Foundation (Grant No. 1665344).

References

1. Baerends EJ (2001) Exact exchange-correlation treatment of dissociated H_2 in density functional theory. Phys. Rev. Lett. 87:133004
2. Buijse MA, Baerends EJ (2002) An approximate exchange-correlation hole density as a functional of the natural orbitals. Mol Phys 100:401
3. Becke AD (2003) A real-space model of nondynamical correlation. J Chem Phys 119:2972
4. Becke AD (2013) Density functionals for static, dynamical, and strong correlation. J. Chem. Phys 138:074109
5. Kong J, Proynov E (2016) Density functional model for nondynamic and strong correlation. J Chem Theory Comput 12:133
6. Janesko BG, Proynov E, Kong J, Scalmani G, Frisch MJ (2017) Practical density functionals beyond the overdelocalization-underbinding zero-sum game. J Phys Chem Lett 8:4314
7. Li C, Zheng X, Cohen AJ, Sanchez PM-, Yang W (2015) Local scaling correction for reducing delocalization error in density functional approximations. Phys. Rev. Lett. 114:053001
8. Chen L, Zheng X, Su NQ, Yang W (2017) Localized orbital scaling correction for systematic elimination of delocalization error in density functional approximations. Nat Sci Review 5:203
9. Su NQ, Li C, Yang W (2018) Describing strong correlation with fractional-spin correction in density functional theory. PNAS 115:9678
10. Lee TJ, Taylor PR (1989) A diagnostic for determining the quality of single-reference electron correlation methods. Int J Quantum Chem Quantum Chem Symp 23:199
11. Janssen CL, Nielsen IMB (1998) New diagnostics for coupled-cluster and moller-plesset perturbation theory. Chem Phys Lett 290:423
12. Karton A, Daon S, Martin JML (2011) W11: a high-confidence benchmark dataset. Chem Phys Lett 510:165
13. Takatsuka K, Fueno T, Yamaguchi K (1978) Distribution of odd electrons in ground-state molecules. Theoret Chim Acta 48:175
14. Lain L, Torre A, Bochicchio RC, Ponec R (2001) On the density matrix of effectively unpaired electrons. Chem Phys Lett 346:283
15. Staroverov VN, Davidson ER (2000) Distribution of effectively unpaired electrons. Chem Phys Lett 330:161
16. Head-Gordon M (2003) Characterizing unpaired electrons from the one-particle density matrix. Chem Phys Lett 372:508
17. Ramos-Cordoba E, Salvador P, Matito E (2016) Separation of dynamic and nondynamic correlation. Phys Chem Chem Phys 18:24015
18. Liu F, Duan C, Kulik HJ (2020) Rapid detection of strong correlation with machine learning for transition-metal complex high-throughput screening. J Phys Chem Lett 11:8067
19. Chai J-D (2012) Density functional theory with fractional orbital occupations. J. Chem. Phys. 136:154104
20. Ramos-Cordoba E, Matito E (2017) Local descriptors of dynamic and nondynamic correlation. J Chem Theory Comput 13:2705
21. Grimme S, Hansen A (2015) A practicable real-space measure and visualization of static electron-correlation effects. Angew Chem Int Ed 54:12308
22. Nakano M, Kishi R, Nitta T et al (2005) Second hyperpolarizability (γ) of singlet diradical system: dependence of γ on the diradical character. J Phys Chem A 109:885
23. Proynov E, Liu F, Kong J (2013) Analysing effects of strong electron correlation within Kohn-Sham Density-functional theory. Phys. Rev. A 88:032510
24. Fukuda K, Nakano M (2014) Intramolecular charge transfer effects on the diradical character character and second Hyperpolarizabilities of open-shell singlet X-pi-X (X= Donor/Acceptor) systems. J Phys Chem A 118:3463
25. Kamada K, Fuku-en S-i, Minamide S et al (2013) Impact of diradical character on two-photon absorption: Bis(acridine) dimers synthesized from an allenic precursor. J Am Chem Soc 135:232
26. Nakano M, Kishi R, Ohta S et al (2007) Relationship between third-order nonlinear optical properties and magnetic interactions in open-shell systems: a new paradigm for nonlinear optics. Phys. Rev. Letters 99:033001
27. Nakano M, Kishi R, Ohta S et al (2006) Origin of the enhancement of the second hyperpolarizability of singlet diradical systems wuth intermediate diradical character. J. Chem. Phys. 138:244306
28. Nakano M, Kubo T, Kamada K et al (2006) Second hyperpolarizabilities of polycyclic aromatic hydrocarbons invoolving phenalenyl radical units. Chem Phys Lett 418:142
29. Nakano M, Nagai H, Fukui H et al (2008) Theoretical study of third-order nonlinear optical properties in square nanographenes with open-shell singlet ground states. Chem Phys Lett 467:120
30. Nagai H, Nakano M, Yoneda K et al (2010) Signature of Multiradical character in second hyperpolarizabilities of rectangular graphene nanoflakes. Chem Phys Lett 489:212
31. Staroverov VN, Davidson ER (2000) Electron distributions in radicals. Int J Quant Chem 77:316
32. Becke AD, Roussel MR (1989) Exchange holes in inhomogeneous systems: a coordinate-space model. Phys Rev A 39:3761
33. Becke AD (2005) Real-space post-Hartree-Fock correlation models. J Chem Phys 122:64101
34. Becke AD (1988) A multicenter numerical integration scheme for polyatomic molecules. J Chem Phys 88:2547
35. Turney JM, Simmonett AC, Parrish RM et al (2012) Psi4: an open-source ab initio electronic structure program. WIRES Comput Mol Sci 2:556
36. Frisch MJ, Trucks GW, Schlegel HB et al (2016) Gaussian development version, Revision I. 11. Gaussian Inc, Wallingford CT
37. Curtiss LA, Raghvachari K, Redfern PC, Rassolov V, Pople JA (1998) Gaussian-3 (G3) theory for molecules containing first and second-row atoms. J Chem Phys 109:7764
38. Liu F, Kong J (2017) An algorithm for efficient computation of exchange energy density with Gaussian basis functions. J Chem Theory Comput 13:2571
39. Liu F, Furlani T, Kong J (2016) Optimal path search for recurrence relation in cartesian Gaussian integrals. J Phys Chem A 120:10264
40. Liu F, Kong J (2018) An efficient implementation of semi-numerical computation of the Hartree-Fock exchange on the Intel Phi processor. Chem Phys Letters 703:106
41. Jiang W, DeYonker NJ, Wilson AK (2012) Multireference character for 3d TM compounds. J Chem Theory Comput 8:460
42. Wang J, Manivasagam S, Wilson AK (2015) Multireference character for 4d transition metal-containing molecules. J Chem Theory Comput 11:5865

43. Fogueri UR, Kozuch S, Karton A, Martin JML (2013) A simple DFT-based diagnostic for nondynamical correlation. Theor Chem Acc 132:1291
44. Schultz NE, Zhao Y, Truhlar DG (2005) Density functionals for inorganometallic and organometallic chemistry. J Phys Chem A 109:11127
45. Lee TJ (2003) Comparison of the T1 and D1 diagnostics for electronicstructure theory: a new definition for the open-shell D1 diagnostic. Chem Phys Lett 372:362
46. Cousins KR (2005) *ChemDraw Ultra 9.0.* J. Am. Chem. Soc 127: 4115
47. Jacquemin D, Femenias A, Chermette H et al (2006) Assessment of several hybrid DFT functionals for the evaluation of bond length alternation of increasingly long oligomers. J Phys Chem A 110:5952
48. Liang SD, Bai YH, Beng B (2006) Peierls instability and persistent current in mesoscopic conducting polymer rings. Phys. Rev. B 74:113304
49. Sawyer DT, Srivatsa GS, Bodini ME, Schaefer WP, Wing RM (1986) Redox chemistry and spectroscopy of toluene-3,4-dithiol (TDTH2) and of its M(TDT)22-/- complexes with zinc(II), copper(II), nickel(II), cobalt(II), iron(II), and manganese(II). Formation of a stable dn-(.cntdot.SR) bond upon oxidation by one electron. J Am Chem Soc 108:936
50. Zuleta JA, Burberry MS, Eisenberg R (1990) Platinum(II) diimine dithiolates New solution luminescent complexes. Coord. Chem. Rev. 97:47
51. Cassoux P, Valade L, Kobayashi H et al (1991) Molecular metals and superconductors derived from metal complexes of 1,3-dithiol-2-thione-4,5-dithiolate (dmit). Coord Chem Rev 110:115
52. Pilato RS, Stiefel EI (1999) Bioinorganic catalysis. In: Bioinorganic Catalysis. Marcel Dekker, New York, pp 81–152
53. Dang L, Yang X, Zhou J, Brothers EN, Hall MB (2012) Computational studies on ethylene addition to nickel bis(dithiolene). J Phys Chem A 116:476
54. Jiang W, DeYonker NJ, Determan JJ, Wilson AK (2011) Toward accurate theoretical thermochemistry of first row transition metal complexes. J Phys Chem A 116:870